



Cyclic Stability of Superelasticity in [001]-Oriented Quenched $\text{Ni}_{44}\text{Fe}_{19}\text{Ga}_{27}\text{Co}_{10}$ and $\text{Ni}_{39}\text{Fe}_{19}\text{Ga}_{27}\text{Co}_{15}$ Single Crystals

E. E. Timofeeva¹ · E. Yu. Panchenko¹ · A. S. Eftifeeva¹ · A. I. Tagiltsev¹ · N. Yu. Surikov¹ · A. B. Tokhmetova¹ · E. I. Yanushonite¹ · M. V. Zherdeva¹ · I. Karaman² · Yu. I. Chumlyakov¹

Received: 5 July 2022 / Revised: 12 September 2022 / Accepted: 22 September 2022 / Published online: 29 November 2022
© The Chinese Society for Metals (CSM) and Springer-Verlag GmbH Germany, part of Springer Nature 2022

Abstract

The study of the influence of the cobalt content on the cyclic stability of superelasticity (SE) was carried out in quenched $\text{Ni}_{44}\text{Fe}_{19}\text{Ga}_{27}\text{Co}_{10}$ and $\text{Ni}_{39}\text{Fe}_{19}\text{Ga}_{27}\text{Co}_{15}$ (at.%) single crystals under compression. It is shown that an increase in the cobalt content leads to embrittlement of the material and a decrease in the cyclic stability of SE. In $\text{Ni}_{44}\text{Fe}_{19}\text{Ga}_{27}\text{Co}_{10}$ single crystals, during the first 20 loading/unloading cycles, the elastic energy relaxation occurs along with the formation of dislocations and residual martensite, which leads to a decrease in critical stress of martensite formation and in stress hysteresis. During the next 80 cycles, SE becomes more stable. Stabilization is accompanied by a slight change in the parameters. On the contrary, $\text{Ni}_{39}\text{Fe}_{19}\text{Ga}_{27}\text{Co}_{15}$ single crystals are characterized by high-strength characteristics, which lead to high SE stability during the first 20 loading/unloading cycles. However, after 20 cycles, a strong degradation of the SE is observed through the formation of microcracks, which ultimately leads to the destruction of the sample. The results of work are replicable for cycling at different temperatures from all temperature ranges of superelasticity.

Keywords Martensitic transformations · Superelasticity · Single crystals · Cyclic stability · Microstructure

1 Introduction

Extensive systematic studies of the shape memory effect (SME) and superelasticity (SE) have been carried out on NiFeGaCo alloys with cobalt content $C_{\text{Co}}=0-6$ at.% [1–3]. NiFeGaCo alloys demonstrated a wide SE temperature range, large strain, and high cyclic stability. These properties make them promising materials for applications. It was revealed that an increase in the cobalt content leads to a decrease in the temperatures of martensitic transformation (MT) [4–6] and complete suppression of thermal-induced MT at a cobalt content of more than 10 at.% [4, 5]. A large number of defects lead to a strong crystal lattice distortion. In this case, instead of MT, a strain glass transition (from unfrozen to frozen strain glass) occurs during cooling. A

strain glass transition is found in many alloys based on Ti–Ni, Ni–Mn–Ga, Ni–Mn–In, and Fe–Pd [7].

Despite the absence of thermal-induced MT in NiFeGaCo alloys with cobalt concentration $C_{\text{Co}} \geq 10$ at.%, it is possible to observe stress-induced MT and, accordingly, SME and SE [4–6]. In our previous work on NiFeGaCo single crystals with $C_{\text{Co}}=10-15$ at.%, it was shown that the cobalt content has a significant effect on the SE. It determines the SE temperature range and the critical stresses of martensite formation. At the same time, the SE cyclic stability in these alloys has not been studied in depth. We are aware of only one work [4]: fibers of $\text{Ni}_{35}\text{Fe}_{18}\text{Ga}_{27}\text{Co}_{20}$ alloy (of ~30–500 μm) demonstrated the SE with narrow hysteresis and high cyclic stability in tension (up to 8000 cycles without significant degradation). The same authors conducted similar experiments on bulk NiFeGaCo polycrystals with $C_{\text{Co}}=10$ and 12 at.% and demonstrated SE with wider hysteresis in compression [5, 6]. Since the stress hysteresis determines the dissipation energy during MT, it should be expected that in bulk materials, where the SE is accompanied by large dissipation energy, the SE cyclic stability will be weaker than in fibers. Moreover, the cobalt content could affect the SE cyclic stability. Thus, the abovementioned questions determine the

Available online at <http://link.springer.com/journal/40195>.

✉ E. E. Timofeeva
timofeeva_katie@mail.ru

¹ Tomsk State University, Novosobornaya Square 1,
Tomsk 634050, Russia

² Texas A&M University, College Station, TX 77843, USA

significance and innovation of present research, which aims to study the influence of the cobalt content on the SE, the critical stresses level, stress hysteresis, and SE cyclic stability in NiFeGaCo single crystals with $C_{Co} = 10$ and 15 at.%.

The [001]-oriented Ni₄₄Fe₁₉Ga₂₇Co₁₀ and Ni₃₉Fe₁₉Ga₂₇Co₁₅ (at.%) single crystals were chosen to study. Our previous works showed that quenched [001]-oriented Ni₄₄Fe₁₉Ga₂₇Co₁₀ (at.%) single crystals undergo thermal-induced MTs upon cooling and demonstrate SE in a wide temperature range from 218 to 473 K with high-strength properties of the B2-phase of 870 MPa in compression [8, 9]. On the contrary, Ni₃₉Fe₁₉Ga₂₇Co₁₅ single crystals did not undergo thermal-induced MTs, and, as follows from literature [4–6], they exhibited a strain glass transition upon cooling. Ni₃₉Fe₁₉Ga₂₇Co₁₅ crystals were characterized by higher martensite formation stresses and a narrower SE temperature range. Thus, this choice will allow us to study the effect of cobalt content on the SE and its cyclic stability taking into account various types of thermal-induced transformations that are observed in crystals (MT and strain glass).

The [001]-orientation was chosen because it is characterized by higher strength properties of austenite and martensite in NiFeGa(Co) single crystals, and, consequently, by the highest cyclic stability compared to other orientations [3]. Under compression along the [001]-orientation, there is no contribution of detwinning of the L1₀-martensite, which ensures low dissipated energy and narrow stress hysteresis and, ultimately, should provide a higher cyclic stability of SE in comparison with other orientations.

2 Materials and Methods

Ni₄₄Fe₁₉Ga₂₇Co₁₀ (at.%) and Ni₃₉Fe₁₉Ga₂₇Co₁₅ (at.%) single crystals were grown by the Bridgman method. The chemical composition was controlled by energy dispersive X-ray spectroscopy on using a scanning microscope electron TESCAN VEGA 3. The composition corresponded to the nominal composition with the error of 5%. All mechanical tests were performed in compression. The compressions samples were parallelepipeds with dimensions of 3 mm × 3 mm × 6 mm. The studies were conducted on as-grown [001]-oriented single crystals and crystals annealed at 1448 K for 1 h followed by quenching in water (called “quenched crystals”). The MT temperatures were investigated by the temperature dependence of the electrical resistance. The SE curves in compression were collected at temperatures from 200 to 500 K with an Instron 5969 testing machine at a strain rate of 10⁻³ s⁻¹. Electron microscopy studies were conducted with Hitachi HT-7700. During the data analysis, the measurement errors of strain ± 0.1%, temperature ± 1 K, and stress ± 2 MPa were taken into account.

3 Results

Figure 1 shows the microstructures of single crystals before mechanical testing. The quenched Ni₄₄Fe₁₉Ga₂₇Co₁₀ and Ni₃₉Fe₁₉Ga₂₇Co₁₅ crystals had single dislocations and no secondary phases (Fig. 1a, c). The selected area diffraction pattern (SADP) with zone axis [011]_{L21} contains <111>_{L21} reflections. The dark-field images obtained from these reflections show antiphase domains separated by dark regions of similar size (Fig. 1b, d). Consequently, in the quenched crystals, austenite is a mixture of B2 and L2₁-phases, which was also observed for NiFeGa alloys [10–12]. The presence of the B2-phase is associated with annealing above the order–disorder L2₁-B2 transition (973 K for NiFeGa [12]). The domain size depends on cobalt concentration and equals to 20–50 nm in Ni₄₄Fe₁₉Ga₂₇Co₁₀ and less than 10 nm in Ni₃₉Fe₁₉Ga₂₇Co₁₅.

The MT temperatures for the Ni₄₄Fe₁₉Ga₂₇Co₁₀ single crystals are as follows: $M_s = 203$ K; $M_f = 163$ K; $A_s = 173$ K; $A_f = 218$ K. In Ni₃₉Fe₁₉Ga₂₇Co₁₅ single crystals, the MTs were not observed in the temperature dependence of the electrical resistance upon cooling to 77 K. Instead, upon cooling, a strain glass transition occurred, which is confirmed by previous results reported in the literature [5, 6].

Figure 2 presents the $\sigma(\epsilon)$ curves upon loading/unloading for the quenched crystals in the SE temperature range.

In Ni₄₄Fe₁₉Ga₂₇Co₁₀ single crystals, SE is observed in a wide temperature range of 255 K (from $A_f = 218$ K to 473 K). In Ni₃₉Fe₁₉Ga₂₇Co₁₅ single crystals, the SE temperature range is shifted up to lower temperatures; therefore, SE is not observed above 348 K. In all single crystals under study, the shape of the SE curves changes with an increase in temperature: stages appear on the curves, critical stress of the martensite formation σ_{cr} increases, the reversible strain ϵ_{rev} decreases and stress hysteresis $\Delta\sigma$ increases. The $\sigma(\epsilon)$ curves show stages with different strain hardening coefficients $\theta = d\sigma/d\epsilon$. The first stage is a stress plateau with a low strain hardening coefficient θ , the second stage with a high θ appears with an increase in the strain degree. The stress plateau and the reversible strain decrease with increasing temperature. This is accompanied by a growth in the strain hardening coefficient $\theta = d\sigma/d\epsilon$ at the second stage. Such a change may be associated with the fact that the martensitic shear occurs at high temperatures and high stress under conditions of high elasticity constants.

Figure 3a shows the dependences of stress hysteresis on the test temperature $\Delta\sigma(T)$ for Ni₄₄Fe₁₉Ga₂₇Co₁₀ and Ni₃₉Fe₁₉Ga₂₇Co₁₅ single crystals. Regardless of the chemical composition, the plots of $\Delta\sigma(T)$ have the same shape: a slight change in hysteresis with increasing temperature is followed by a sharp increase in hysteresis.

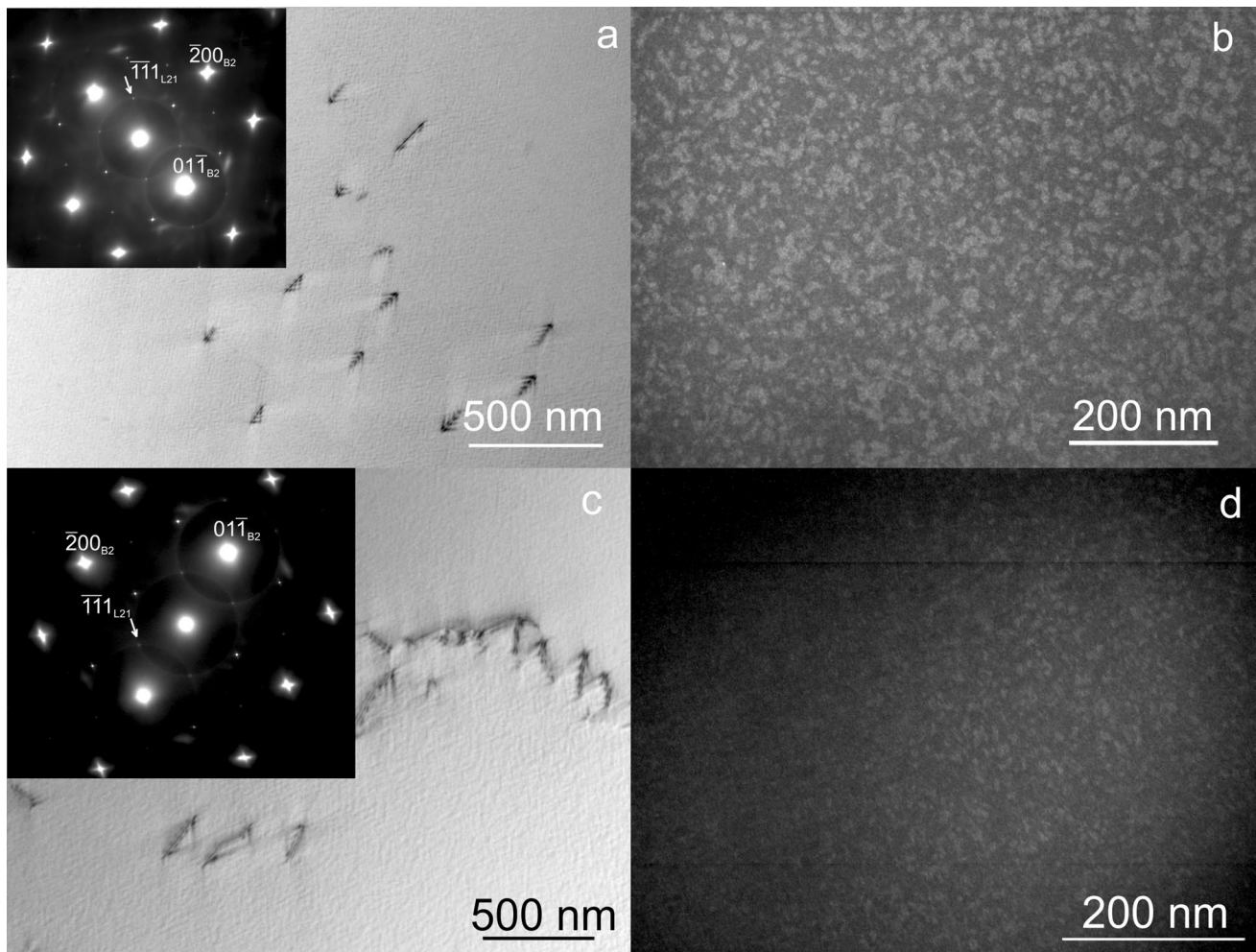


Fig. 1 Microstructures of quenched $\text{Ni}_{44}\text{Fe}_{19}\text{Ga}_{27}\text{Co}_{10}$ **a, b** and $\text{Ni}_{39}\text{Fe}_{19}\text{Ga}_{27}\text{Co}_{15}$ **c, d** single crystals: **a, c**—bright-field images and corresponding SADPs, matrix zone axis is $[011]_{L21}$; **b, d**—dark-field images in $\langle 111 \rangle_{L21}$ reflections

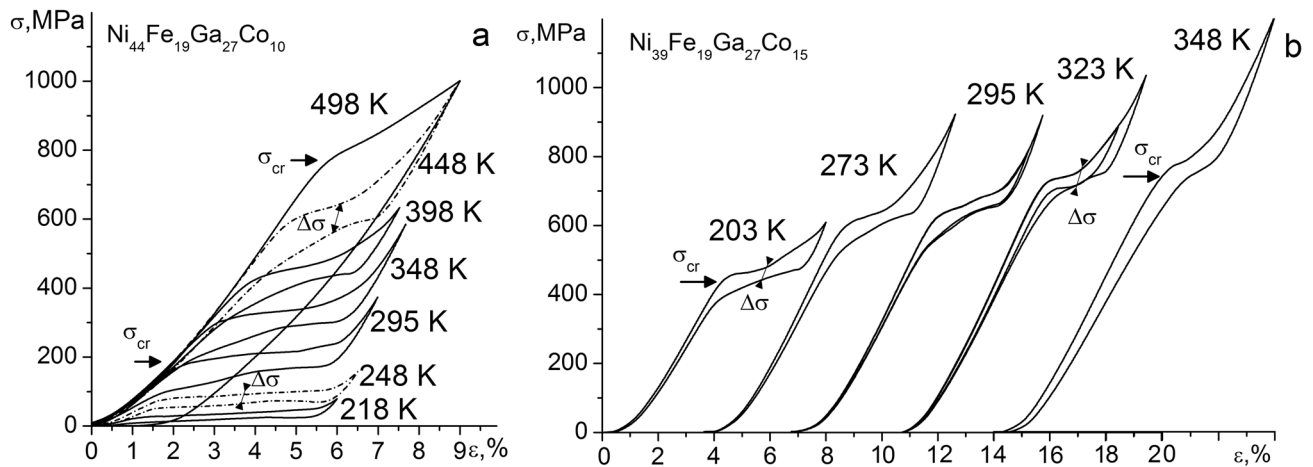


Fig. 2 $\sigma(\varepsilon)$ response for quenched $\text{Ni}_{44}\text{Fe}_{19}\text{Ga}_{27}\text{Co}_{10}$ **a** and $\text{Ni}_{39}\text{Fe}_{19}\text{Ga}_{27}\text{Co}_{15}$ **b** crystals

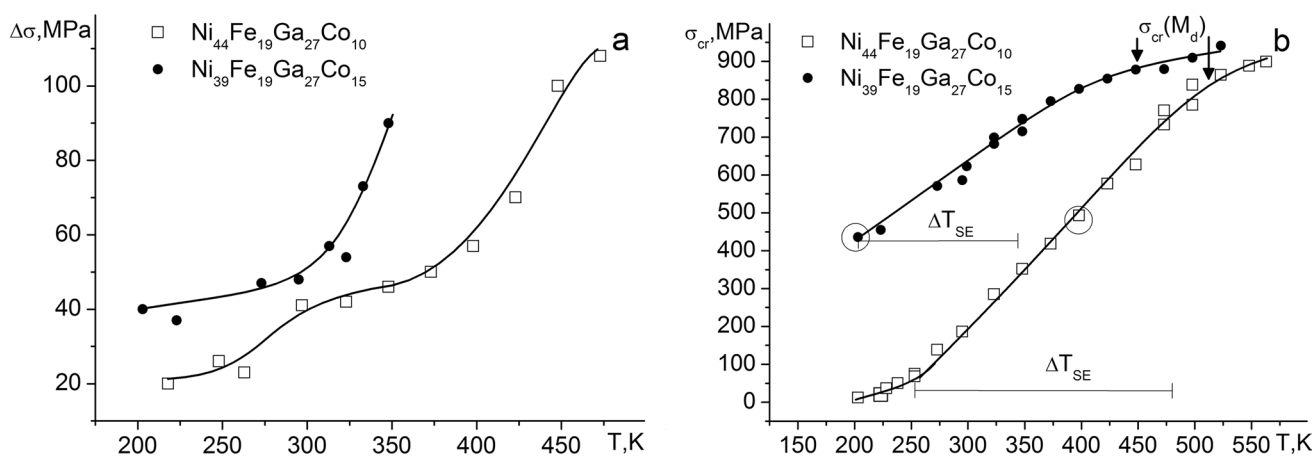


Fig. 3 Temperature dependences of stress hysteresis **a** and critical stress **b** for quenched Ni₄₄Fe₁₉Ga₂₇Co₁₀ and Ni₃₉Fe₁₉Ga₂₇Co₁₅ single crystals. The circles indicate the conditions for cyclic tests

The sharp increase is associated with approaching the yield strength of austenite and a sharp increase in the generation of defects during the MT. The weak dependence of hysteresis on the test temperature is associated with the absence of detwinning under a compressive stress applied along the [001]-direction. In such a case, according to Roitburd [13], an increase in the stresses does not change the twinning structure of martensite and the orientation of the habit plane, and hence the dissipated energy and stress hysteresis are constant. In other cases where detwinning is present, for example, in tension along the [001]-orientation or in compression along the [011]-direction, stress hysteresis increases significantly (up to 10 times) with increasing test temperature. At the same time, there is a bend at the stage of a slight change in hysteresis for Ni₄₄Fe₁₉Ga₂₇Co₁₀ single crystals (Fig. 3a). The bend was also observed in [001]-oriented NiFeGa and NiFeGaCo single crystals in compression and was associated with a change in the MT sequence from L2₁-14 M to L2₁-L1₀ [3]. In Ni₄₄Fe₁₉Ga₂₇Co₁₀ single crystals, the sequence of MT is likely to change. In Ni₃₉Fe₁₉Ga₂₇Co₁₅ single crystals, such a bend was not observed.

Critical stresses of martensite formation on the $\sigma(\epsilon)$ curves increase with increasing temperature (Fig. 3b), in accordance with the Clausius–Clapeyron relation [3]. Stress increases up to the yield strength level of the high-temperature phase $\sigma_{cr}(M_d)$, which equals to 840 MPa for Ni₄₄Fe₁₉Ga₂₇Co₁₀ and 905 MPa for Ni₃₉Fe₁₉Ga₂₇Co₁₅ crystals. The strength properties of the high-temperature phase limit the SE temperature range, which ranges from 250 to 475 K in Ni₄₄Fe₁₉Ga₂₇Co₁₀ single crystals and from 200 to 350 K in Ni₃₉Fe₁₉Ga₂₇Co₁₅ single crystals.

Based on the presented experimental data, it can be concluded that an increase in the cobalt content (with a decrease in nickel) leads, firstly, to an increase in the

resistance of the matrix to the formation of oriented martensite, which is manifested in an increase in the stresses required for the formation of martensite; secondly, an increase in cobalt content causes a slight increase in strength properties of matrix. These changes are likely to have a significant effect on the SE cyclic stability. In Ni₃₉Fe₁₉Ga₂₇Co₁₅ crystals, the temperature dependence of the critical stresses is strongly shifted relative to the temperature dependence in Ni₄₄Fe₁₉Ga₂₇Co₁₀ crystals (Fig. 3b). Then, the close thermodynamic conditions were chosen to study the cyclic stability, namely a close value of the nonchemical Gibbs energy $\Delta G_{\text{nonch}} = \Delta G_{\text{rev}} + \Delta G_{\text{irr}}$ and close critical stresses for the martensite formation. At these conditions, the stress level for the existence of martensite is far from the yield strength of austenite by similar values for Ni₄₄Fe₁₉Ga₂₇Co₁₀ and Ni₃₉Fe₁₉Ga₂₇Co₁₅ single crystals. When choosing one test temperature, the Ni₄₄Fe₁₉Ga₂₇Co₁₀ crystals are characterized by low critical stress level, whereas the Ni₃₉Fe₁₉Ga₂₇Co₁₅ crystals demonstrated high stress level close to the yield strength properties. Thus, the plastic deformation can be observed during MT in the Ni₃₉Fe₁₉Ga₂₇Co₁₅ crystals, whereas this effect will not occur in Ni₄₄Fe₁₉Ga₂₇Co₁₀ alloys. Based on the conditions, the test temperatures were chosen to be 398 K in Ni₄₄Fe₁₉Ga₂₇Co₁₀ single crystals and 203 K in Ni₃₉Fe₁₉Ga₂₇Co₁₅ single crystals. Figure 4 shows the $\sigma(\epsilon)$ curves during 100 loading/unloading cycles. Cycling was carried out up to 700 MPa in order to avoid plastic deformation.

The SE cyclic stability strongly depends on the cobalt content. Figure 5 shows the dependences of the critical stresses σ_{cr} , stress hysteresis $\Delta\sigma$, and strain hardening coefficient $\theta = d\sigma/d\epsilon$ on the number of cycles. In Ni₄₄Fe₁₉Ga₂₇Co₁₀ single crystals, these dependences can be divided into two steps (Fig. 5a–c).

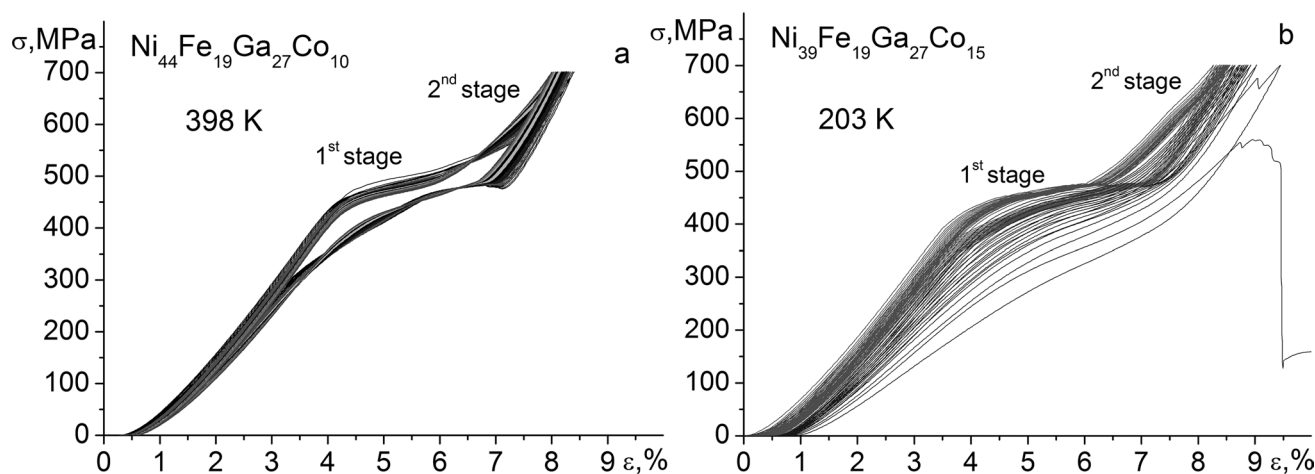


Fig. 4 $\sigma(\varepsilon)$ response during 1–100 cycles for quenched $\text{Ni}_{44}\text{Fe}_{19}\text{Ga}_{27}\text{Co}_{10}$ **a** and $\text{Ni}_{39}\text{Fe}_{19}\text{Ga}_{27}\text{Co}_{15}$ **b** single crystals

The maximum degradation of the SE loop occurred in the first 20 cycles, when the critical stresses σ_{cr} decrease by 5%, and stress hysteresis decreases by 35%. The second step, 21–100 cycles, is characterized by more stable SE: stresses decrease by only 3%, and stress hysteresis decreases by 15%. The total accumulated strain during 100 cycles did not exceed 0.3%. The strain hardening coefficient $\theta = d\sigma/d\varepsilon$, which was measured for the stress plateau stage on the $\sigma(\varepsilon)$ curve, remained unchanged for 100 cycles. However, at the stage of stress growth, the coefficient $\theta = d\sigma/d\varepsilon$ increased from 60×10^2 to 90×10^2 MPa within 30 cycles and then changed slightly.

In $\text{Ni}_{39}\text{Fe}_{19}\text{Ga}_{27}\text{Co}_{15}$ single crystals, the dependences of critical stress σ_{cr} and hysteresis $\Delta\sigma$ on the number of cycles have a different shape (Fig. 5d–f). During the first 20 cycles, as in $\text{Ni}_{44}\text{Fe}_{19}\text{Ga}_{27}\text{Co}_{10}$ single crystals, stresses and hysteresis decreased by 4% and 11%, respectively. It should be noted that in the first 20 cycles in $\text{Ni}_{39}\text{Fe}_{19}\text{Ga}_{27}\text{Co}_{15}$ single crystals, the changes in parameters were less than in $\text{Ni}_{44}\text{Fe}_{19}\text{Ga}_{27}\text{Co}_{10}$. However, after 20 cycles, instead of stability, strong degradation of SE occurred. As a result, cycles 21–29 saw the stress decrease by 35% and stress hysteresis increase by 240%. After 29 cycles, sample destruction occurs. Depending on the sample, the number of cycles before fracture (fatigue life) varies by no more than 10 cycles and can be associated with various structural imperfections in different samples.

The total accumulated irreversible strain from cycles 1–29 was 0.8%. The strain hardening coefficient $\theta = d\sigma/d\varepsilon$, which was measured for the stress plateau stage on the $\sigma(\varepsilon)$ curve, changed slightly up to cycle 20, but doubled from cycle 20 to cycle 29. On the contrary, at the stage of stress growth, the coefficient $\theta = d\sigma/d\varepsilon$ did not change.

4 Discussion

In the works [14, 15], the authors proposed to describe the SE cyclic stability based on the ratio of the elastic ΔG_{rev} and the dissipated ΔG_{irr} energy during the stress-induced MT. The energy values ΔG_{rev} and ΔG_{irr} per unit volume are calculated from loading/unloading cycles as the area inside the $\sigma(\varepsilon)$ curve and the area under the unloading curve, respectively [15, 16]. The ratio of elastic and dissipated energies $\Delta G_{\text{rev}}/\Delta G_{\text{irr}}$ characterizes the relationship between critical stresses σ_{cr} , stress hysteresis $\Delta\sigma$, reversible strain ε_{rev} , and irreversible strain ε_{irr} . It was shown in literature [14] that in $\text{Ni}_{49}\text{Fe}_{18}\text{Ga}_{27}\text{Co}_6$ single crystals, the high SE stability is observed if the $\Delta G_{\text{rev}}/\Delta G_{\text{irr}}$ ratio is high, and vice versa. This depends on the microstructure and orientation.

In the present work, the values of ΔG_{rev} and ΔG_{irr} and their ratio for $\text{Ni}_{44}\text{Fe}_{19}\text{Ga}_{27}\text{Co}_{10}$ and $\text{Ni}_{39}\text{Fe}_{19}\text{Ga}_{27}\text{Co}_{15}$ single crystals were estimated based on $\sigma(\varepsilon)$ curves during cycling. Figure 6 illustrates the values of ΔG_{rev} and ΔG_{irr} and their ratio depending on the number of cycles. Chemical composition influences the shape of dependences. In $\text{Ni}_{44}\text{Fe}_{19}\text{Ga}_{27}\text{Co}_{10}$ single crystals, the elastic and dissipated energies decrease with an increase in the number of cycles, which is consistent with [16]. In this case, the elastic energy ΔG_{rev} decreases smoothly and uniformly with an increase in the number of cycles by 7%. The dissipated energy ΔG_{irr} decreases sharply in the first 10 cycles, and then it gradually decreases by 2.3 times in the next 90 cycles. Taking into account that the elastic energy significantly exceeds the dissipated energy, as a result, their ratio increases by a factor of 2 with an increase in the number of cycles.

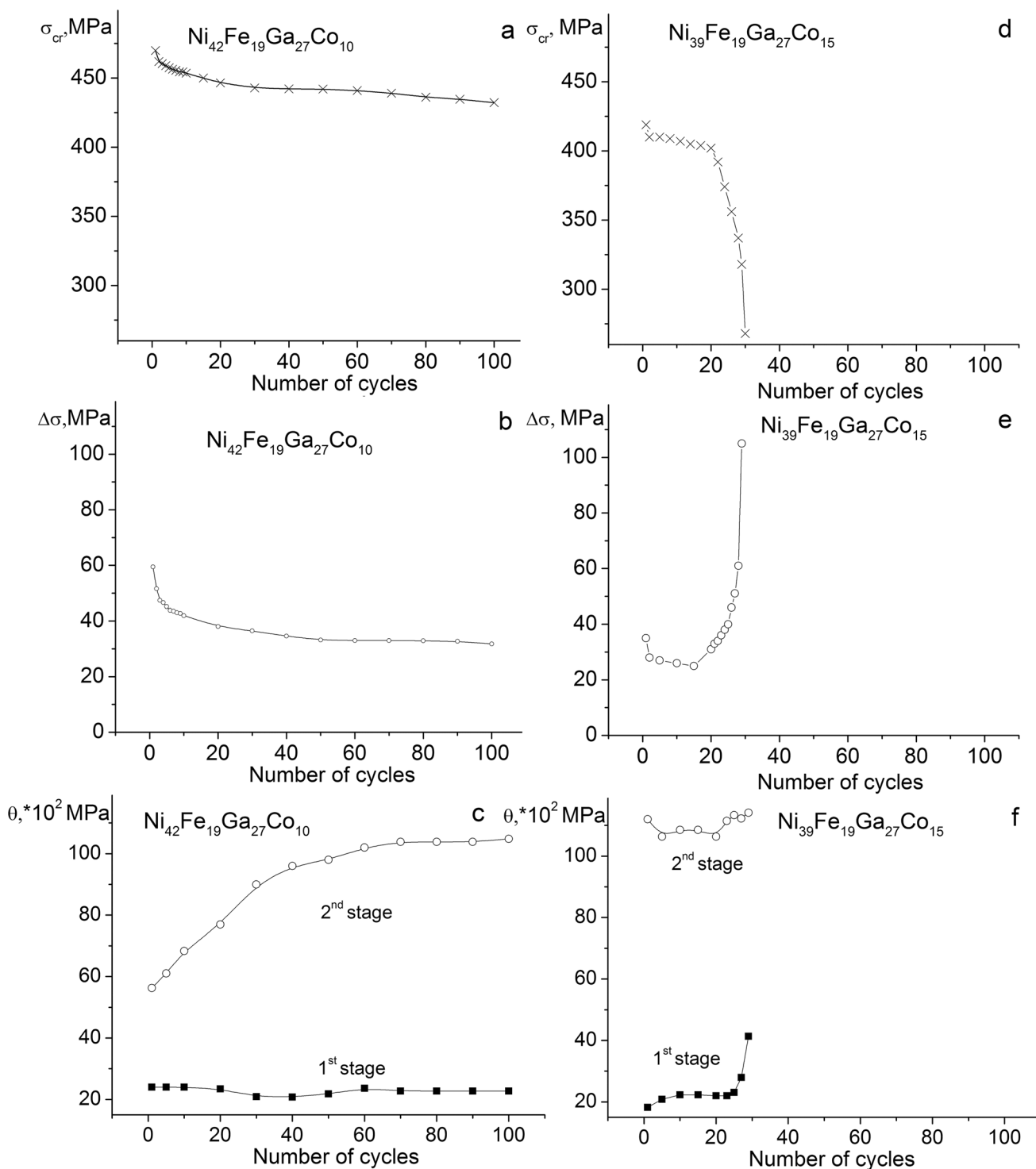


Fig. 5 Dependences of critical stress σ_{cr} **a, d** of stress hysteresis $\Delta\sigma$ **b, e** and strain hardening coefficient $\theta=d\sigma/d\varepsilon$ **c, f** on the number of cycles for quenched Ni₄₄Fe₁₉Ga₂₇Co₁₀ **a-c** and Ni₃₉Fe₁₉Ga₂₇Co₁₅ **d-f** single crystals

On the contrary, in Ni₃₉Fe₁₉Ga₂₇Co₁₅ single crystals, the elastic and dissipated energies change nonmonotonically. The elastic energy ΔG_{rev} , which slightly increased before cycle 20, sharply decreases by 12% after 20 cycles.

Dissipated energy, which is initially reduced by 1.4 times, increases sharply by 2.5 times after 20 cycles. As a result, the ratio of elastic and dissipated energies $\Delta G_{rev}/\Delta G_{irr}$

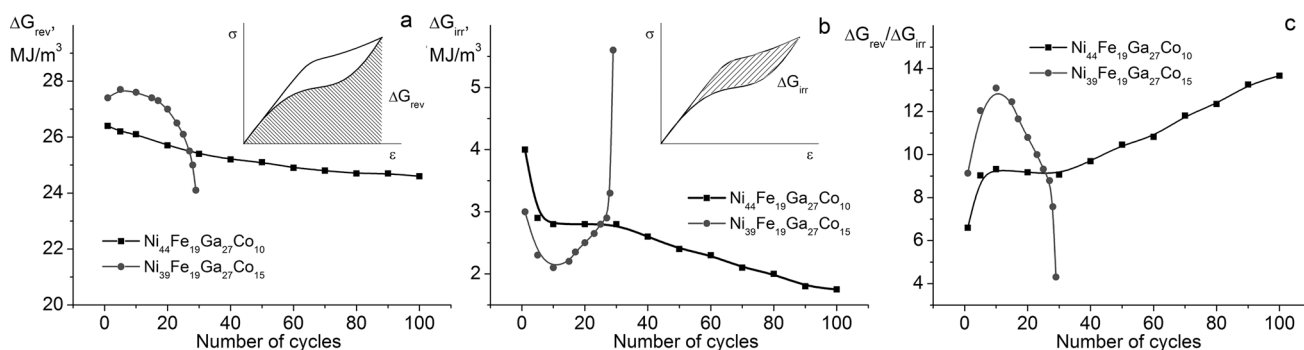


Fig. 6 Estimation of elastic energy ΔG_{rev} **a**, dissipated energy ΔG_{irr} **b** and their ratio $\Delta G_{\text{rev}}/\Delta G_{\text{irr}}$ **c**

increases by 1.5 times during the first 20 cycles and then sharply decreases by 3.2 times from 20 to 29 cycles.

Thus, dependencies presented in Fig. 6 can be divided into two steps: the first 20 cycles and subsequent cycles. It can be seen from Figs. 4, 5, and 6 that the degradation in the first 20 cycles in $\text{Ni}_{44}\text{Fe}_{19}\text{Ga}_{27}\text{Co}_{10}$ single crystals is more pronounced than in $\text{Ni}_{39}\text{Fe}_{19}\text{Ga}_{27}\text{Co}_{15}$. In $\text{Ni}_{44}\text{Fe}_{19}\text{Ga}_{27}\text{Co}_{10}$ single crystals, in the first 20 cycles, the elastic energy is lower, the dissipated energy is higher, and the ratio $\Delta G_{\text{rev}}/\Delta G_{\text{irr}}$ is lower than in $\text{Ni}_{39}\text{Fe}_{19}\text{Ga}_{27}\text{Co}_{15}$ crystals. This means that in $\text{Ni}_{44}\text{Fe}_{19}\text{Ga}_{27}\text{Co}_{10}$ single crystals, less accumulation of elastic energy occurs with its more active dissipation.

The functional degradation that occurs in the first 20 cycles in $\text{Ni}_{44}\text{Fe}_{19}\text{Ga}_{27}\text{Co}_{10}$ single crystals consists in the relaxation of the elastic energy near the austenite/martensite interface due to the formation of dislocations, residual martensite, and martensite stabilization [14, 17]. In this case, a decrease in critical stress was observed, since in each subsequent cycle martensite will nucleate on defects left after the previous one [17, 18]. The effect of dislocation

and residual martensite in $\text{Ni}_{44}\text{Fe}_{19}\text{Ga}_{27}\text{Co}_{10}$ single crystals can be traced through an additional study of the SME in the stress-assisted cooling/heating cycles (Fig. 7a). For this, a stress of 100 MPa was chosen, when the maximum volume fraction of oriented martensite and the maximum strain of 4.1% were observed. It has been established that after cyclic tests, the temperatures of the start of stress-induced MT increased by ~20 K. This indicates the presence of internal elastic stress fields that contribute to the formation of oriented martensite, lower the critical stresses of the start of MT, and increase the MT temperature. The magnitude of these stresses in $\text{Ni}_{44}\text{Fe}_{19}\text{Ga}_{27}\text{Co}_{10}$ single crystals can be estimated from the temperature shift M_s^σ (at 100 MPa) in accordance with the Clausius–Clapeyron equation [3]:

$$\Delta M_s^\sigma(\sigma) = -(\epsilon_{\text{tr}}/\Delta S) < \sigma_G >, \quad (1)$$

where ϵ_{tr} is the transformation strain, ΔS is the entropy change. The estimate gives 30–60 MPa. In addition to defects and residual martensite, the above effect in $\text{Ni}_{44}\text{Fe}_{19}\text{Ga}_{27}\text{Co}_{10}$ single crystals can be due to partial

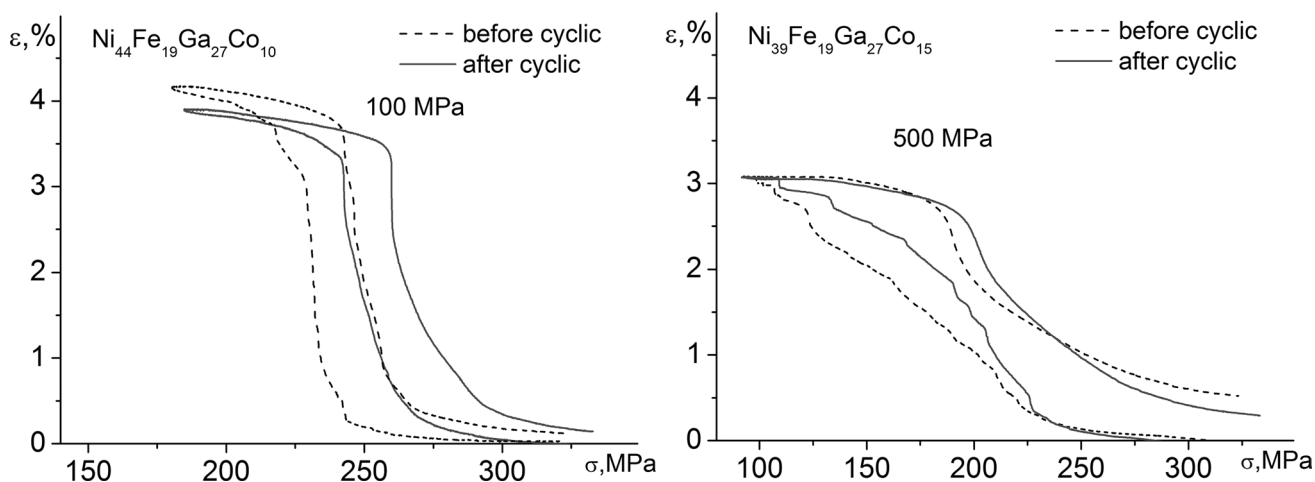


Fig. 7 $\epsilon(T)$ curves before and after cyclic tests for quenched $\text{Ni}_{44}\text{Fe}_{19}\text{Ga}_{27}\text{Co}_{10}$ (100 cycles) and $\text{Ni}_{39}\text{Fe}_{19}\text{Ga}_{27}\text{Co}_{15}$ (18 cycles) single crystals

stabilization of martensite, which occurs at elevated temperatures due to diffusion processes associated with the redistribution of point defects and the arrangement of atoms of different types in accordance with the martensite symmetry during testing. In work [19] on NiFeGaCo alloys, the effect of martensite stabilization under similar conditions on the SME and SE was shown.

A different situation was observed in Ni₃₉Fe₁₉Ga₂₇Co₁₅ single crystals. In the first 20 cycles, SE degraded less compared to Ni₄₄Fe₁₉Ga₂₇Co₁₀ crystals: stress hysteresis changed by only 11% versus 35%, and strain hardening coefficient $\theta = d\sigma/d\varepsilon$ did not change. Figure 6 shows that in Ni₃₉Fe₁₉Ga₂₇Co₁₅ single crystals, the elastic energy is higher, the dissipated energy is lower, and the energy ratios $\Delta G_{\text{rev}}/\Delta G_{\text{irr}}$ are larger than in Ni₄₄Fe₁₉Ga₂₇Co₁₀ single crystals. Therefore, it can be assumed that a more significant accumulation of elastic energy occurred in Ni₃₉Fe₁₉Ga₂₇Co₁₅ single crystals (Fig. 6). Elastic energy was not dissipated into the formation of defects and residual martensite. Therefore, in Ni₃₉Fe₁₉Ga₂₇Co₁₅ single crystals, the $\varepsilon(T)$ curves in stress-assisted cooling/heating cycles, obtained after 18 cycles, coincided with the initial curves before testing (Fig. 7b).

An additional experiment was carried out on Ni₄₄Fe₁₉Ga₂₇Co₁₀ and Ni₃₉Fe₁₉Ga₂₇Co₁₅ single crystals at the same temperature in order to exclude the influence of different temperatures, as well as cold brittleness as the reason for the increased brittleness of Ni₃₉Fe₁₉Ga₂₇Co₁₅ samples. The room temperature is optimal for this experiment. At 298 K, Ni₄₄Fe₁₉Ga₂₇Co₁₀ single crystals demonstrate the SE, and Ni₃₉Fe₁₉Ga₂₇Co₁₅ single crystals have the critical stresses lower than the yield point of austenite. The curves $\sigma(\varepsilon)$ during cycling and the dependences of critical stresses and hysteresis on the number of cycles are shown in Fig. 8.

This experiment confirms the data obtained on the basis of the previous experiment at various temperatures (Figs. 4

and 5). First, in the Ni₄₄Fe₁₉Ga₂₇Co₁₀ single crystals, a similar degradation of the SE is observed during the first 20 cycles at 298 K (σ_{cr} decreases by 5%, $\Delta\sigma$ decreases by 35%), as in the case of cycling at an elevated temperature of 398 K. With an increase in the number of cycles above 20, in the Ni₄₄Fe₁₉Ga₂₇Co₁₀ single crystals, SE degrades weakly up to 500 cycles, as well as at 398 K. Secondly, the Ni₃₉Fe₁₉Ga₂₇Co₁₅ single crystals demonstrate the weak degradation of the SE at 298 K in the first 10 cycles (σ_{cr} decreases by 1%, $\Delta\sigma$ decreases by 15%). However, after 42 cycles, a sharp degradation of the SE is observed (σ_{cr} decreases by 20%, $\Delta\sigma$ increases by 500%) and samples destructed after 46 cycles. Depending on the sample, fatigue life of the Ni₃₉Fe₁₉Ga₂₇Co₁₅ single crystals at 298 K is 30–50 cycles, which is close to fatigue life at 203 K.

Thus, the experiments made it possible to cover a wide temperature range in Ni₄₄Fe₁₉Ga₂₇Co₁₀ and Ni₃₉Fe₁₉Ga₂₇Co₁₅ single crystals. Cycling was carried out at low and high temperatures associated with the beginning and the end of the SE temperature range, respectively. It allows us to state that the results of this work will be replicable when cycling at other temperatures.

Different degradation in Ni₄₄Fe₁₉Ga₂₇Co₁₀ and Ni₃₉Fe₁₉Ga₂₇Co₁₅ single crystals can be associated with different strength properties of martensite at the selected test temperatures. Figure 9 shows $\sigma(\varepsilon)$ curves with the yield strength of martensite at temperatures near the cycling temperatures.

It can be seen that the yield strength of 1360 MPa in Ni₄₄Fe₁₉Ga₂₇Co₁₀ single crystals at 373 K is much lower than in Ni₃₉Fe₁₉Ga₂₇Co₁₅ crystals, where it is 1805 MPa at 213 K. Such a difference in the strength properties is associated with a decrease in the yield strength with increasing temperature, which is typical of NiFeGa(Co) alloys [20].

As it was mentioned above, no thermal-induced MTs were found in Ni₃₉Fe₁₉Ga₂₇Co₁₅ single crystals during stress-free

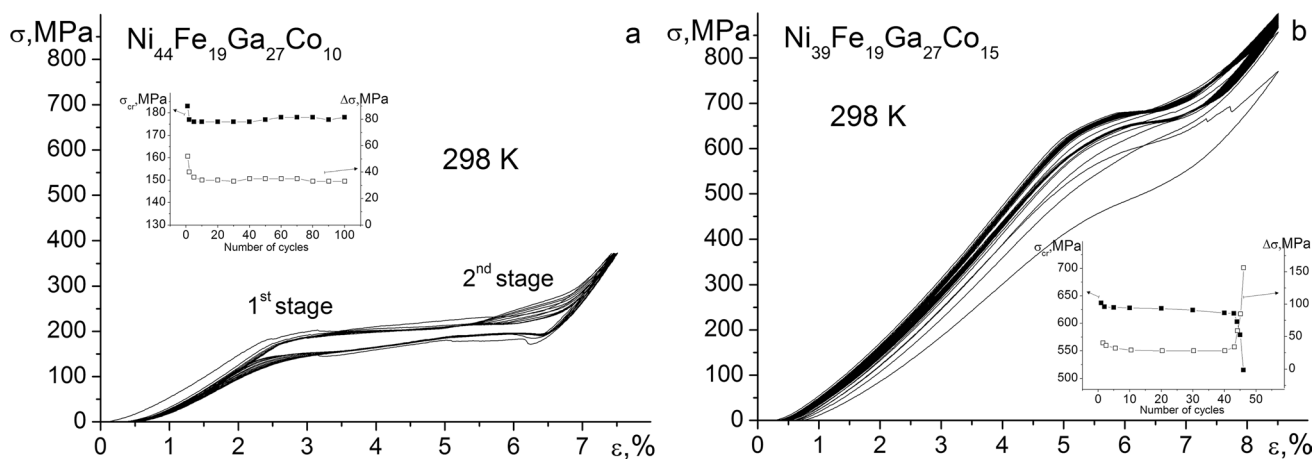


Fig. 8 $\sigma(\varepsilon)$ response during cycling for quenched Ni₄₄Fe₁₉Ga₂₇Co₁₀ **a** and Ni₃₉Fe₁₉Ga₂₇Co₁₅ **b** single crystals at 298 K

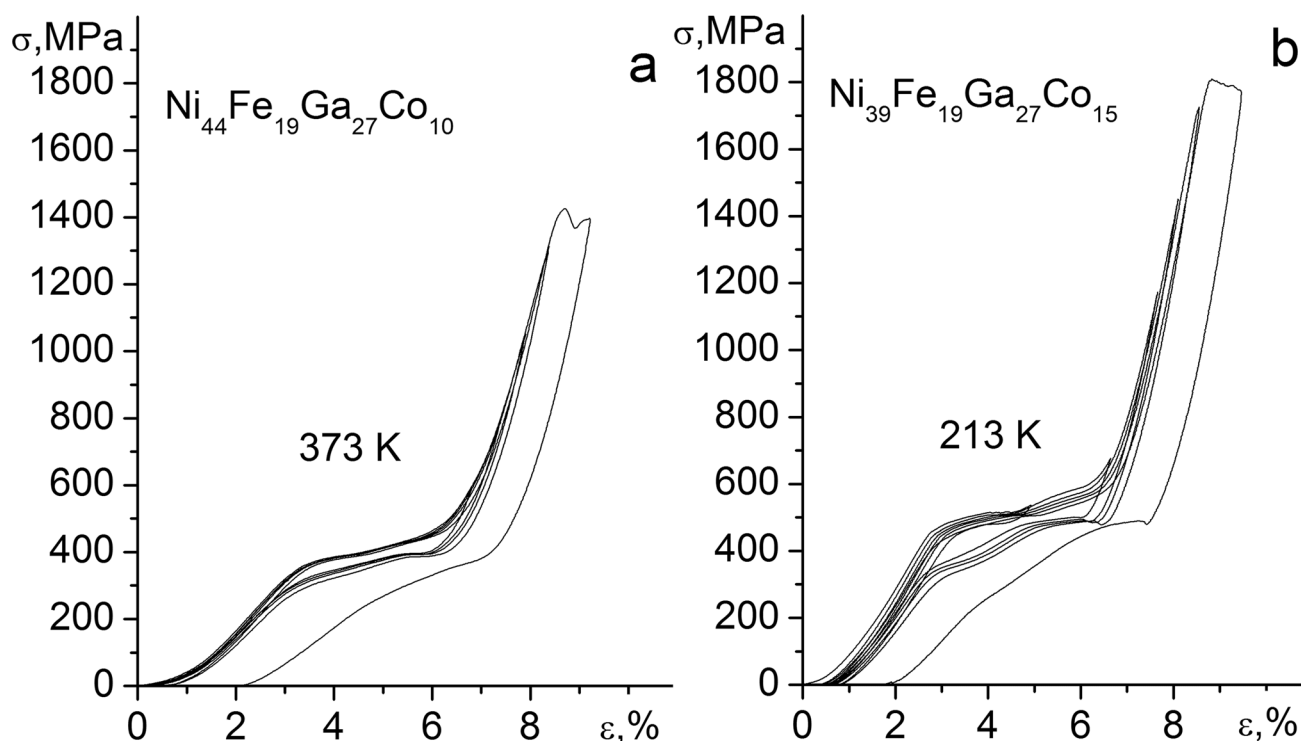


Fig. 9 $\sigma(\varepsilon)$ curves under compressive load for quenched $\text{Ni}_{44}\text{Fe}_{19}\text{Ga}_{27}\text{Co}_{10}$ and $\text{Ni}_{39}\text{Fe}_{19}\text{Ga}_{27}\text{Co}_{15}$ single crystals demonstrating the yield strength of $L1_0$ -martensite at temperatures of 213 K and 373 K

cooling/heating. Based on the literature data, in NiFeGaCo with such cobalt content, a strain glass transition was observed due to a large number of point defects that prevent the formation of martensite macrolamellae and form nanodomains with a local order. A strain glass transition was found in many alloys based on Ti–Ni, Ni–Mn–Ga, Ni–Mn–In, and Fe–Pd [7]. At the same time, it was found that in these alloys, stress-induced MT can be observed at a high stress level. Indeed, Fig. 2 demonstrates that it is necessary to apply stresses much higher than in $\text{Ni}_{44}\text{Fe}_{19}\text{Ga}_{27}\text{Co}_{10}$ crystals to obtain stress-induced martensite in $\text{Ni}_{39}\text{Fe}_{19}\text{Ga}_{27}\text{Co}_{15}$ crystals. Consequently, $\text{Ni}_{39}\text{Fe}_{19}\text{Ga}_{27}\text{Co}_{15}$ crystals are characterized by a high resistance of the matrix to the growth of oriented martensite. It can be assumed that such a special microstructure in $\text{Ni}_{39}\text{Fe}_{19}\text{Ga}_{27}\text{Co}_{15}$ is the reason for the accumulation of large elastic energy during the formation of finely dispersed martensite under stress. This is indirectly confirmed by Fig. 7, where the large temperature intervals of MT are observed in $\text{Ni}_{39}\text{Fe}_{19}\text{Ga}_{27}\text{Co}_{15}$ single crystals. The value of temperature intervals is proportional to the value of the elastic energy accumulated during the MT [21, 22].

The behavior of single crystals under cyclic loads in the first 20 cycles also determined SE response in subsequent cycles in $\text{Ni}_{44}\text{Fe}_{19}\text{Ga}_{27}\text{Co}_{10}$ single crystals. After 20 cycles, the degradation decreased and the SE became more stable, the decrease in critical stresses and stress hysteresis, and

the increase in the coefficient $\theta = d\sigma/d\varepsilon$ slowed down. In this case, the ratio of elastic and dissipated energy increases monotonically all the time. This may be due to dislocation hardening during the first cycles. On the contrary, in $\text{Ni}_{39}\text{Fe}_{19}\text{Ga}_{27}\text{Co}_{15}$ single crystals, a strong relaxation of the elastic energy was observed after 20 cycles. Consequently, there was no formation of a large number of defects and hardening, and an increase in local stress led to microcracks and degradation. Therefore, after 20 cycles at 203 K $\text{Ni}_{39}\text{Fe}_{19}\text{Ga}_{27}\text{Co}_{15}$ single crystals showed a significant increase in stress hysteresis (by 240%), reduction in critical stress of martensite formation (35%), and a sharp increase in the strain hardening coefficient at the first stage of the curve $\sigma(\varepsilon)$ (2 times) (Fig. 5). Figure 10 a, b illustrates the surface samples after 18 and 25 loading/unloading cycles, when microcracks begin to form and grow rapidly with a repeated number of cycles. Similar tests in $\text{Ni}_{44}\text{Fe}_{19}\text{Ga}_{27}\text{Co}_{10}$ single crystals did not lead to microcracks, but, on the contrary, left traces of plastic deformation.

As a result, the subsequent cycling of $\text{Ni}_{39}\text{Fe}_{19}\text{Ga}_{27}\text{Co}_{15}$ single crystals led to brittle fracture, as evidenced by the fractography of the cleavage surface (Fig. 10 c, d). The destruction of $\text{Ni}_{44}\text{Fe}_{19}\text{Ga}_{27}\text{Co}_{10}$ single crystals under selected cycling conditions at 398 K up to 700 MPa did not reveal during first 500 cycles. The reason for the brittleness of $\text{Ni}_{39}\text{Fe}_{19}\text{Ga}_{27}\text{Co}_{15}$ single crystals, compared with

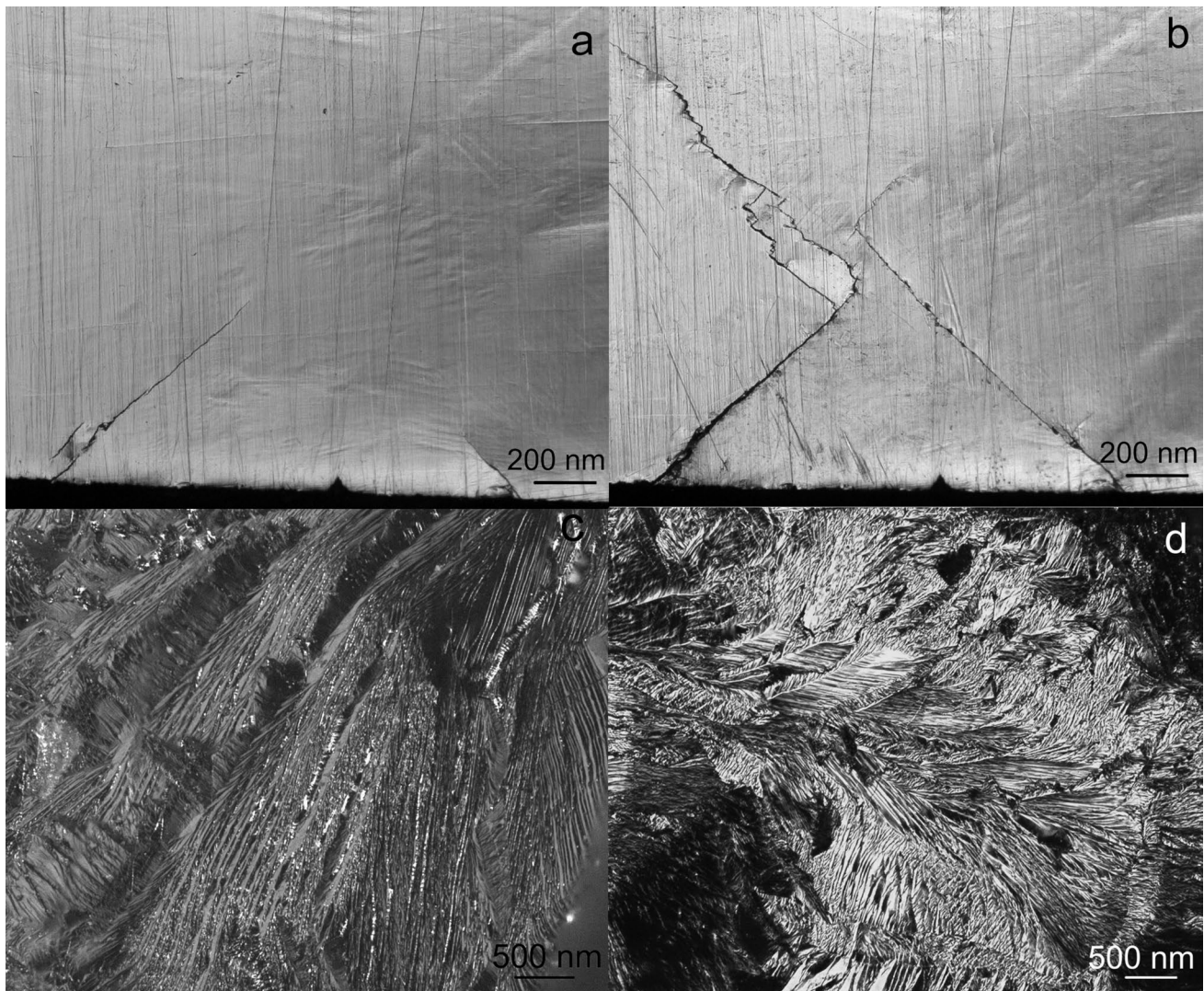


Fig. 10 Optical metallography of the surface after 18 loading/unloading cycles **a** and after 25 cycles **b**; fractography of the fracture surface after 29 cycles **c**, **d** in Ni₃₉Fe₁₉Ga₂₇Co₁₅ single crystals, cycling temperature 203 K

Ni₄₄Fe₁₉Ga₂₇Co₁₀ crystals, is an increase in the cobalt content, which causes not only an increase in the resistance of the matrix to the formation of oriented martensite and an increase in strength properties, but also leads to an increase in brittleness and a decrease in plasticity.

5 Conclusions

The effect of the cobalt content on the stress hysteresis, the level of critical stresses, and the SE cyclic stability in quenched Ni₄₄Fe₁₉Ga₂₇Co₁₀ and Ni₃₉Fe₁₉Ga₂₇Co₁₅ (at.%) single crystals under compressive stress was experimentally established. It has been established that the dependence of the SE cyclic stability on the cobalt content changes slightly with a change in the test temperature within the SE

temperature range. It was established that SE degradation occurred in two steps.

In Ni₄₄Fe₁₉Ga₂₇Co₁₀ single crystals, at the first step (1–20 cycles), the elastic energy relaxed with the formation of dislocations and residual martensite, which led to a decrease in the critical stresses of martensite formation (by 5%), a reduction in hysteresis (by 35%), and an increase in the strain coefficient hardening (1.5 times). At the second step of degradation (20–100 cycles), in Ni₄₄Fe₁₉Ga₂₇Co₁₀ single crystals, SE became more stable, which was accompanied by a slight change in the parameters. Fatigue life of Ni₄₄Fe₁₉Ga₂₇Co₁₀ single crystals is more than 500 cycles.

On the contrary, Ni₃₉Fe₁₉Ga₂₇Co₁₅ single crystals with a higher cobalt content were characterized by higher strength characteristics of austenite and martensite, which led to higher stability during the first 20 loading/unloading cycles

compared to $\text{Ni}_{44}\text{Fe}_{19}\text{Ga}_{27}\text{Co}_{10}$ single crystals; there was a decrease in critical stresses (by 4%), a reduction in hysteresis values (by 11%), and there was not an increase in the strain hardening coefficient. After 20 cycles, $\text{Ni}_{39}\text{Fe}_{19}\text{Ga}_{27}\text{Co}_{15}$ single crystals showed strong SE degradation through the formation of microcracks: a decrease in critical stresses (by 35%), a decrease in the hysteresis value (by 240%), and an increase in the strain hardening coefficient (2 times). As a result, this led to the destruction of single crystals. Fatigue life of $\text{Ni}_{39}\text{Fe}_{19}\text{Ga}_{27}\text{Co}_{15}$ single crystals does not exceed 46 cycles.

Acknowledgements This work was financially supported by the Russian Science Foundation (No. 21-19-00287). The electron microscopy studies were carried out on the equipment of the Krasnoyarsk Regional Center for Collective Use SB RAS.

References

- [1] F. Masdeu, J. Pons, J. Torrens-Serra, Y. Chumlyakov, E. Cesari, *Mater. Sci. Eng. A* **833**, 142362 (2022)
- [2] F. Masdeu, J. Pons, Y. Chumlyakov, E. Cesari, *Mater. Sci. Eng. A* **805**, 140543 (2021)
- [3] Y.I. Chumlyakov, I.V. Kireeva, E.Y. Panchenko, E.E. Timofeeva, I.V. Kretinina, O.A. Kuts, in *Shape memory alloys: properties, technologies, opportunities*. ed. by N. Resnina, V. Rubanik (Trans Tech. Publications Ltd, 2015)
- [4] H. Chen, Y.D. Wang, Z. Nie, R. Li, D. Cong, W. Liu, F. Ye, Y. Liu, P. Cao, F. Tian, X. Shen, R. Yu, L. Vitos, M. Zhang, S. Li, X. Zhang, H. Zheng, J.F. Mitchell, Y. Ren, *Nat. Mater.* **19**, 712 (2020)
- [5] D.P. Wang, X. Chen, Z.H. Nie, *Europhys. Lett.* **98**, 46004 (2012)
- [6] Q.H. Zhang, Z. Zhai, Z.H. Nie, S. Harjo, D.Y. Cong, M.G. Wang, J. Lie, Y.D. Wang, *J. Appl. Cryst.* **48**, 1183 (2015)
- [7] X. Sun, D. Cong, Y. Ren, K.D. Liss, D.E. Browne, Z. Ma, S. Hao, W. Xia, Z. Chena, L. Ma, X. Zhaoli, Z. He, J. Liug, R. Li, Y. Wang, *Acta Mater.* **183**, 11 (2020)
- [8] E.E. Timofeeva, EYu. Panchenko, A.S. Eftifeeva, A.I. Tagiltsev, NYu. Surikov, A.B. Tokhmetova, E.I. Yanushonite, M.V. Zherdeva, I. Karaman, Yu.I. Chumlyakov, *AIP Conf Proc.* **2509**, 020191 (2022)
- [9] E.E. Timofeeva, EYu. Panchenko, M.V. Zherdeva, Yu.I. Chumlyakov, I. Karaman, *Mat. Lett.* **310**, 131477 (2022)
- [10] T. Omori, N. Kamiya, Y. Sutou, K. Oikawa, R. Kainuma, K. Ishida, *Mater. Sci. Eng. A* **378**, 403 (2004)
- [11] K. Oikawa, T. Ota, T. Ohmori, Y. Tanaka, H. Morito, A. Fujita, R. Kainuma, K. Fukamichi, K. Ishida, *Appl. Phys. Lett.* **81**, 5201 (2002)
- [12] R. Santamarta, E. Cesari, J. Font, J. Muntasell, J. Pons, J. Dutkiewicz, *Scr. Mater.* **54**, 1985 (2006)
- [13] A.F. Manchón-Gordón, J.J. Ipus, M. Kowalczyk, M. Kowalczyk, A. Wojcik, J.S. Blazquez, C.F. Conde, W. Maziarz, P. Svec, T. Kulik, A. Conde, *J. Alloys Compd.* **844**, 156092 (2020)
- [14] E.E. Timofeeva, EYu. Panchenko, N.G. Vetoshkina, Yu.I. Chumlyakov, A.I. Tagiltsev, A.S. Eftifeeva, H. Maier, *Russ. Phys. J.* **59**, 1251 (2016)
- [15] M.J. Mahtabi, N. Shamsaei, *Int. J. Mech. Sci.* **117**, 321 (2016)
- [16] Y. Zhang, Y. You, Z. Moumni, G. Anlas, J. Zhu, W. Zhang, *Smart Mater. Struct.* **28**, 065027 (2019)
- [17] C. Lauhoff, A. Reul, D. Langenkämper, P. Krooß, C. Somsen, M.J. Gutmann, B. Pedersen, I.V. Kireeva, Y.I. Chumlyakov, G. Eggeler, W.W. Schmahl, T. Niendorf, *Acta Mater.* **226**, 117623 (2022)
- [18] C. Yu, G. Kang, Q. Kan, *J. Mech. Phys. Solids* **82**, 97 (2015)
- [19] EYu. Panchenko, E.E. Timofeeva, Yu.I. Chumlyakov, K.S. Osipovich, A.I. Tagiltsev, G. Gerstein, H.J. Maier, *Mater. Sci. Eng. A* **746**, 448 (2019)
- [20] E.E. Timofeeva, EYu. Panchenko, Yu.I. Chumlyakov, H.J. Maier, G. Gerstein, *Tech. Phys. Lett.* **43**, 320 (2017)
- [21] D.L. Beke, L. Daróczy, N.M. Samy, L.Z. Tóth, M.K. Bolgár, *Acta Mater.* **200**, 490 (2020)
- [22] N.M. Samy, L. Daróczy, L.Z. Tóth, E. Panchenko, Y. Chumlyakov, N. Surikov, D.L. Beke, *Metals* **10**, 534 (2020)

Springer Nature or its licensor (e.g. a society or other partner) holds exclusive rights to this article under a publishing agreement with the author(s) or other rightsholder(s); author self-archiving of the accepted manuscript version of this article is solely governed by the terms of such publishing agreement and applicable law.